$E4$ properties in deformed nuclei and the *sdg* interacting boson model

H. C. Wu,* A. E. L. Dieperink, and O. Scholten
Kernfysisch Versneller Instituut, 9747 AA Groningen, The Netherlands

M. N. Harakeh
Natuurkundig Laboratorium, Vrije Universiteit, 1007 MC Amsterdam, The Netherlands

R. De Leo
University of Bari, Bari, Italy

M. Pignanelli
University of Milan, Milan, Italy

I. Morrison
University of Melbourne, Parkville, Victoria, Australia
(Received 9 June 1988)

The hexadecapole transition strength distribution is measured for the deformed nucleus ^{150}Nd using the (p,p') reaction at $E_p = 30$ MeV. The experimental information on $B(E4)$ values in this nucleus and in ^{156}Gd is interpreted in the framework of the *sdg* interacting boson model. It is found that the main features of the experimental data are fairly well reproduced by a Hartree-Bose method plus Tamm-Dancoff approximation.

I. INTRODUCTION

The interacting boson model (IBA)[1] has been shown to provide a simple phenomenological description of collective properties of nuclei away from closed shells. Microscopically[2] the s and d bosons in the standard model have been interpreted as the image of collective nucleon pairs with angular momentum $J=0$ and 2, respectively. Some microscopic studies have shown[3] that for observable quantities such as moments of inertia, quadrupole moments, etc., in deformed nuclei the effect of higher L pairs, especially the G pair ($L=4$), cannot be neglected. Although in most cases in the boson space the effect of g bosons can be absorbed into the s- and d-boson parameters,[4] there are cases that the g-boson degree of freedom is needed explicitly. For this reason an *sdg* IBA model was introduced[5-7] in which s, d, and g bosons are treated on equal footing. In this way the presence of odd-K bands[5,6] in deformed nuclei, the quenching of $B(E2)$ value[6] and $M1$ properties,[8] etc., could be explained.

It is the aim of the present paper to investigate the role of the g boson for hexadecapole properties in which the role of the $L=4$ pair is expected to show up most directly. To investigate the role of the g boson first $E4$ transition probabilities will be analyzed. The $E4$ transition probabilities are most directly influenced by the g boson and the strength of its coupling to the s-d boson system. Experimental information on hexadecapole transition rates is rather limited; in the rare-earth region data to $E_x \sim 2.5$ MeV have been reported only for the deformed nucleus ^{156}Gd (Ref. 9). In order to obtain information on $E4$ strength distributions in a transitional nucleus, a (p,p') experiment was performed at the Kerntysisch Versheller Instituut (KVI) on the nucleus ^{150}Nd. A common feature of the experimental $E4$ strength distribution is its large fragmentation. While the $E4$ transition to the first 4^+ state is the strongest, the remaining strength is distributed over a large number of states. This feature cannot be explained by the standard *sd* IBA model,[1] since there are only three low-lying 4^+ states that carry $E4$ strength. In Ref. 10, where the effect of the coupling of a single g boson to the *sd* core was studied for ^{156}Gd, the $E4$ strength was predicted to be concentrated in three states in the energy region $E_x = 1.5 \sim 2.3$ MeV. In the present paper we report on a study of $E4$ properties with no restriction on the number of g bosons.

Section II contains a description of the analysis of the experimental data. In Sec. III, $E4$ properties of deformed nuclei are discussed in the SU(3) limit of the *sdg* model. In this limit the energy of the g boson is taken to be degenerate with those of the s and d bosons, giving rise to a maximal mixing of the different boson species. A more realistic situation, corresponding to a perturbed SU(3) Hamiltonian is studied in Sec. IV by employing the Hartree-Bose plus Tamm-Dancoff approximation (HB+TDA) method. Section V contains a microscopic description of the systematics of the hexadecapole moments. The influence of the g boson on other physical observables is studied in Sec. VI. Section VII includes the discussion and the conclusions.

II. EXPERIMENTAL PROCEDURE AND DETERMINATION OF HEXADECAPOLE STRENGTH

A. Experimental procedure and results

The experimental procedure and results for the ^{156}Gd(p,p') reaction have been discussed in Ref. 9 and

will not be repeated here. However, the data for ^{150}Nd(p,p') reaction have been obtained recently and will be discussed briefly.

A 30.3 MeV proton beam from the KVI azimuthially varying field (AVF) cyclotron was used to bombard a ^{150}Nd target of 1.2 mg/cm^2 thickness and 93% isotopic enrichment. The scattered protons were detected by means of the QMG/2 magnetic spectrograph[11] using the newly installed[12] two-dimensional multiwire detection chamber (MWDC). The spectrograph solid angle was set to $\Delta\Omega=4.3$ msr with horizontal opening angle of $\Delta\theta=2.5°$. Spectra were measured for angles ranging from 12° to 80° in steps of 4°. For each angle spectra were obtained for two magnetic field settings: one to obtain cross sections for the elastic and low-lying inelastic peaks at a reduced beam current and another setting at a lower field so that the elastic peak did not hit the detector. A spectrum at $\theta_{lab}=32°$ taken with the lower field setting is shown in Fig. 1. The spectrum shows rich structure up to 3.5 MeV excitation. The overall energy resolution was 12 keV. This was still not good enough to resolve much of the structure above 2 MeV. Therefore, the spectra were analyzed using a multipeak fitting program. Angular distributions were determined for many peaks up to about 3.5 MeV excitation energy. Absolute differential cross sections were determined by normalizing elastic differential cross sections to predictions of optical-model calculations. The uncertainties in the differential cross sections due to this normalization procedure are estimated to be less than 5%. The differential cross sections were compared to distorted-wave Born approximation (DWBA) calculations (as will be discussed shortly) to determine the multipolarity and strength of the transitions. Since in this paper we are only interested in hexadecapole strength, we show in Fig. 2 differential cross sections for two representative hexadecapole transitions, the magnitudes of which differ by almost a factor of 10.

B. CC and DWBA analysis: Determination of hexadecapole strength

For the 4^+ state of the ground-state band (gsb) in ^{150}Nd which is strongly coupled to the other members of the gsb it is essential for the determination of the transition strength to perform coupled-channel (CC) calculations to remove contributions of multistep excitations. The calculations in the axial rotor model were performed for the gsb with the program ECIS (Ref. 13) using the optical-model potential parameters (in the usual notation): $V=53.8$ MeV, $r_R=1.154$ fm, $a_R=0.782$ fm, $W=3.73$ MeV, $W_D=7.3$ MeV, $r_I=1.266$ fm, $a_I=0.723$ fm, $V_{so}=6.0$ MeV, $r_{so}=1.01$ fm, $a_{so}=0.75$ fm, and $r_c=1.2$ fm. Good fits (not shown here) to the differential cross sections of the 0^+, 2^+, and 4^+ states of the gsb were obtained with $\beta_2=0.25$ and $\beta_4=0.059$.

For other hexadecapole transitions at higher excitation energies, which are not strongly coupled to other states, it was sufficient to perform DWBA calculations using

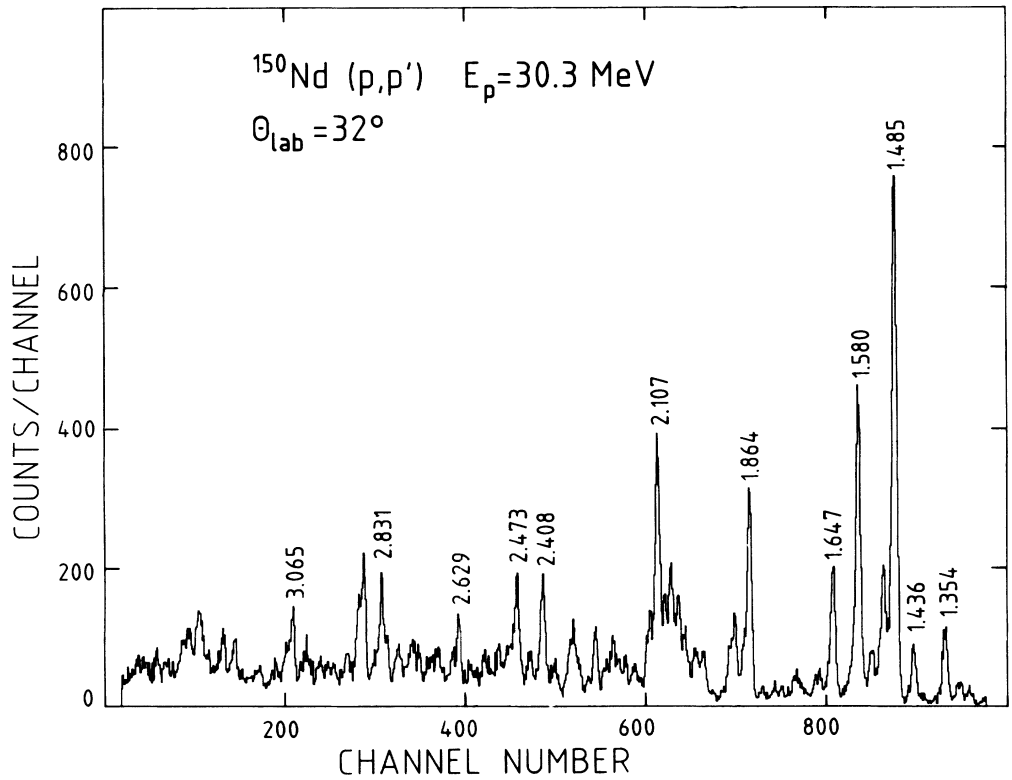

FIG. 1. A spectrum of ^{150}Nd at $\theta_{lab}=32°$ taken with the lower field setting of the *QMG/2* magnetic spectrograph. Some peaks have been labeled with their excitation energies in MeV.

collective transition potentials of the usual first derivative type (RdU/dr) to obtain good fits to the data. This is shown in Fig. 2 for the hexadecapole transitions at 1.647 and 2.704 MeV. By comparing the differential cross sections to the calculated DWBA cross sections deformation parameters β_4 could be obtained.

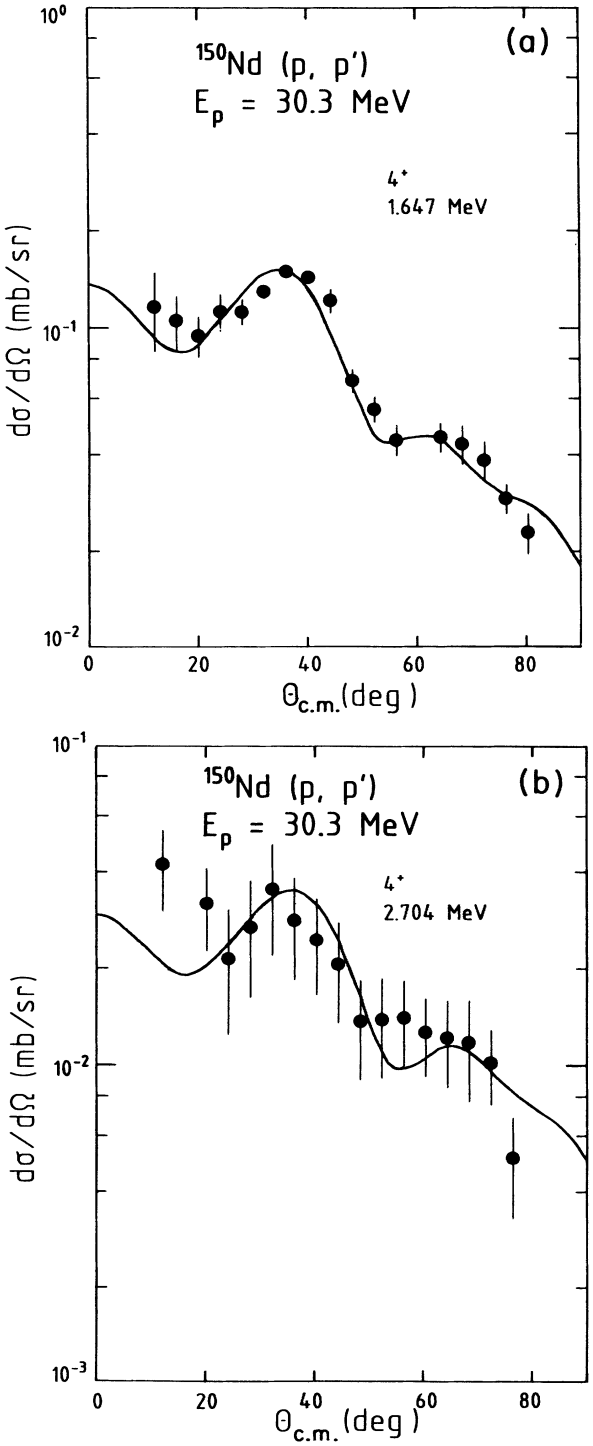

FIG. 2. (a) and (b) Differential cross sections for two representative hexadecapole transitions observed in an inelastic proton scattering.

Hexadecapole transition rates [$B(E4)$ values] for various hexadecapole transitions observed in the experiments on ^{156}Gd and ^{150}Nd were determined from the deformation parameters by evaluating[14] the radial and multipole moments of the real part of the optical-model potentials. Inclusion of the multipole and radial moments of the imaginary parts has little influence on the values of $B(E4)$'s for ^{156}Gd, the differential cross sections of which were analyzed with an optical-model potential with only a volume imaginary term, but has large effects (of about 40%) on the $B(E4)$ values of ^{150}Nd because of the presence of a strong surface imaginary term with a large radial moment in the optical-model potential used. Since in this paper we are only interested in the relative values of the hexadecapole transition rates, the $B(E4)$ values as determined above are plotted in Fig. 3.

III. $E4$ STRENGTH DISTRIBUTION IN THE SU(3) LIMIT OF THE sdg IBA MODEL

The advantage of the study of limiting cases is that results can be obtained analytically. For deformed nuclei, the appropriate limit is the SU(3) limit with the Hamiltonian[6]

$$H=\kappa Q^{(2)}\cdot Q^{(2)}+\kappa' L^{(1)}\cdot L^{(1)}\,, \tag{3.1}$$

where the SU(3) quadrupole operator is given by[6]

$$Q^{(2)}_{\mu}=(d^{\dagger}s+s^{\dagger}\tilde{d})^{(2)}_{\mu}-\tfrac{11}{28}\sqrt{10}(d^{\dagger}\tilde{d})^{(2)}_{\mu}$$
$$+\tfrac{9}{7}(d^{\dagger}\tilde{g}+g^{\dagger}\tilde{d})^{(2)}_{\mu}-\tfrac{3}{14}\sqrt{55}(g^{\dagger}\tilde{g})^{(2)}_{\mu}\,,$$

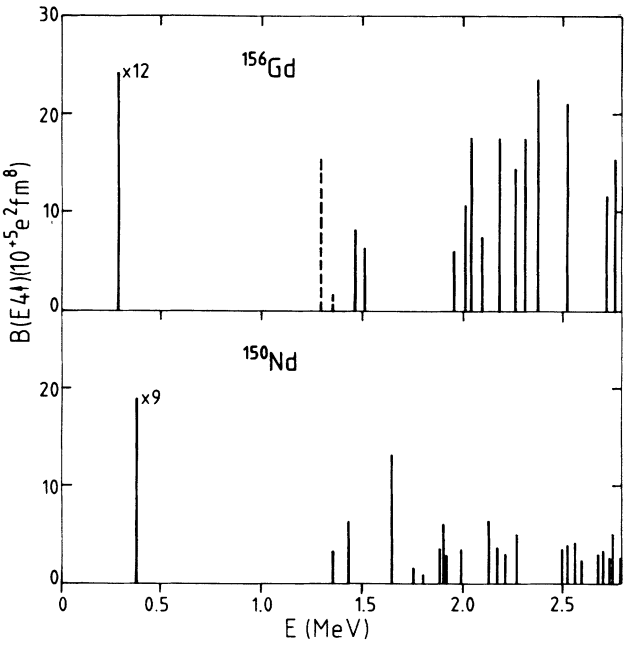

FIG. 3. The experimental 4^+ states and corresponding $B(E4)$ strengths of ^{156}Gd and ^{150}Nd. The $B(E4)$ value for the 4^+ state of the g.s. band must be multiplied with a factor of 12 and 9, respectively, as is indicated in the figure.

and the angular momentum operator by

$$L_\mu^{(1)}=\sqrt{60}(g^\dagger\tilde{g})_\mu^{(1)}+\sqrt{10}(d^\dagger\tilde{d})_\mu^{(1)} . \tag{3.2}$$

In the following subsections the solutions of this Hamiltonian will be discussed, using the intrinsic-state formalism.

A. Intrinsic states in the SU(3) limit

For the calculation of observables in the laboratory system it is convenient to use SU(3) intrinsic states[15] of the *sdg* IBA model. In particular, in the limit of boson number $N\to\infty$ the matrix elements in the laboratory frame can be expressed as intrinsic matrix elements times a geometric factor (as in the geometric collective model). If we restrict ourselves to the irreducible representations (irreps) (λ,μ) of SU(3) with $\mu\le 4$, and to the excitations in which at most one deformed boson is excited, there are eight SU(3) intrinsic states,[15] as discussed in the Appendix.

The most general one-body $E4$ operator can be expressed as

$$T_\mu(E4)=\alpha_0(g^\dagger s+s^\dagger\tilde{g})_\mu^{(4)}+\alpha_1(d^\dagger\tilde{d})_\mu^{(4)} +\alpha_2(d^\dagger\tilde{g}+g^\dagger\tilde{d})_\mu^{(4)}+\alpha_3(g^\dagger\tilde{g})_\mu^{(4)} . \tag{3.3}$$

For the calculation of the transition from the $L=0$ ground state with $\lambda=4N,\mu=0$ to the various excited 4^+ states we need the intrinsic matrix elements $\langle \mathrm{IS}\,|\,T(E4)\,|\,\mathrm{gsb}\rangle$, where $|\,\mathrm{IS}\rangle$ stands for a specific intrinsic state. In Table I, the analytic expressions of those matrix elements for the four terms in Eq. (3.3) are given separately. One sees that the matrix elements within the g.s. band are proportional to N while all others are proportional to $\sqrt{N}$. This implies that for large boson numbers the $E4$ transitions within gsb dominate over the interband transitions. For not too large values of N, there is still a considerable amount of strength going to the other levels. We note that this feature is observed in the experimental data, both in ^{156}Gd and ^{150}Nd.

B. The structure of $E4$ operator

Since the $E4$ operator (unlike the $Q^{(2)}$ operator) is not an SU(3) generator, the choice for the parameters in Eq. (3.3) is still an open question. One possibility to obtain an estimate for the parameters in the $E4$ operator is to use a microscopic model for the bosons. We will first discuss the N dependence of the parameters. Most parameters in the IBA model have a specific mass dependence, including those in the $E4$ operator which accounts for some residual effects introduced by the Pauli principle. One approach that gives particularly simple predictions for this mass dependence is based on the assumption that the IBA states are the image of fermion pair states in the seniority scheme; in particular, this means that one can equate the number of paired fermions in the seniority scheme to the number of s bosons. Using the well-known seniority reduction formulas one obtains, following a procedure that is completely analogous to that given in Ref. 2,

$$\alpha_0(N)\sim\sqrt{(\Omega-N)/(\Omega-1)}$$

and (3.4)

$$\alpha_1^{(N)},\alpha_2^{(N)},\alpha_3^{(N)}\sim\frac{\Omega-2N}{\Omega-2} .$$

The fact that the parameter α_0, in front of the $(s^\dagger\tilde{g}+g^\dagger s)$ term in (3.3), thus has a different N dependence than those in front of the other terms suggests the following parametrization for the $E4$ operator:

$$T^{(E4)}=e_4\{(s^\dagger\tilde{g}+g^\dagger s) +\beta[\eta_1(d^\dagger\tilde{d})^{(4)}+\eta_2(d^\dagger\tilde{g}+g^\dagger\tilde{d})^{(4)} +\eta_3(g^\dagger\tilde{g})^{(4)}]\} , \tag{3.5}$$

where the N dependence of e_4, the hexadecapole effective charge of the bosons, is the same as that of α_0 [see Eq. (3.4)], and where all other N dependence of the parameters is absorbed in β $(\Omega\gg 1)$,

$$\beta(N)\sim\frac{\Omega-2N}{\sqrt{(\Omega-N)\Omega}} . \tag{3.6}$$

The other parameters η_1, η_2, and η_3 are assumed to be N independent. The operator (3.3) can thus be applied to a series of different nuclei with varying e_4 and β, but keeping the parameters η_i constant. Although care needs to be taken when using mappings of operators inconsistent

TABLE I. $E4$ matrix elements in the SU(3) limit. The various intrinsic states are defined in the Appendix.

$\|\,\mathrm{IS}\rangle$	$(s^\dagger\tilde{g}+g^\dagger\tilde{s})^{(4)}$	$(d^\dagger\tilde{d})^{(4)}$	$(d^\dagger\tilde{g}+g^\dagger\tilde{d})^{(4)}$	$(g^\dagger\tilde{g})^{(4)}$
$\|\,\mathrm{gsb}\rangle$	$\frac{4}{5}\sqrt{2/7}N$	$\frac{12}{7}\sqrt{2/35}N$	$-\frac{16}{7}\sqrt{2/77}N$	$\frac{72}{35}\sqrt{2/7\cdot11\cdot13}\cdot N$
$\|\beta\rangle$	$-\frac{2}{5}\sqrt{2/21}\sqrt{N}$	$\frac{6}{7}\sqrt{2/3\cdot35}\sqrt{N}$	$\frac{20}{7}\sqrt{2/3\cdot77}\sqrt{N}$	$-\frac{72}{35}\sqrt{6/7\cdot11\cdot13}\sqrt{N}$
$\|\gamma\rangle$	$\sqrt{6/35}\sqrt{N}$	$\frac{1}{7}\sqrt{6/7}\sqrt{N}$	$-\frac{2}{7}\sqrt{6/5\cdot7\cdot11}\sqrt{N}$	$-\frac{2}{7}\sqrt{66/13\cdot35}\sqrt{N}$
$\|K1\rangle$	$\sqrt{3/35}\sqrt{N}$	$-\frac{4}{7}\sqrt{3/7}\sqrt{N}$	$-\frac{13}{7}\sqrt{3/5\cdot7\cdot11}\sqrt{N}$	$\frac{18}{7}\sqrt{3/11\cdot13\cdot35}\sqrt{N}$
$\|K3\rangle$	$-\sqrt{1/5}\sqrt{N}$	0	$-\sqrt{1/55}\sqrt{N}$	$6\sqrt{1/5\cdot11\cdot3}\sqrt{N}$
$\|g0\rangle$	$\frac{11}{5}\sqrt{1/21}\sqrt{N}$	$-\frac{24}{7}\sqrt{1/3\cdot35}\sqrt{N}$	$\frac{4}{7}\sqrt{1/11\cdot21}\sqrt{N}$	$\frac{36}{35}\sqrt{3/7\cdot11\cdot13}\sqrt{N}$
$\|g2\rangle$	$-\sqrt{1/35}\sqrt{N}$	$\frac{6}{7}\sqrt{1/7}\sqrt{N}$	$\frac{44}{7}\sqrt{1/5\cdot7\cdot11}\sqrt{N}$	$\frac{2}{7}\sqrt{11/13\cdot35}\sqrt{N}$
$\|g4\rangle$	$\sqrt{1/5}\sqrt{N}$	0	$4\sqrt{1/55}\sqrt{N}$	$4\sqrt{1/5\cdot11\cdot13}\sqrt{N}$

with the underlying Hamiltonian (e.g., a seniority mapping in the deformed region), as will be seen below, the first-order results are roughly equivalent to a plausible deformed operator.

To obtain a zeroth-order estimate for the parameters η_i we use the simplest possible choice, namely the prediction of the single j-shell model. In this case one approximates the full major shell by a single j shell with the same multiplicity. The 50–82 major shell, for example, is replaced by a single $j=\frac{31}{2}$ orbit. In this case the parameters η_i (taking $\beta=1$) can be expressed as

$$\eta_1=5\sqrt{2j+1}\begin{Bmatrix}2 & 2 & 4\\ j & j & j\end{Bmatrix}, \tag{3.7a}$$

a similar expression can be derived for η_2 and η_3,

$$\eta_2=3\sqrt{5}\sqrt{2j+1}\begin{Bmatrix}2 & 4 & 4\\ j & j & j\end{Bmatrix}$$

and (3.7b)

$$\eta_3=9\sqrt{2j+1}\begin{Bmatrix}4 & 4 & 4\\ j & j & j\end{Bmatrix}.$$

For $j=\frac{31}{2}$, we obtain $\eta_1=1.18$, $\eta_2=-1.08$, and $\eta_3=1.03$. For realistic multi-j cases one of course expects deviations from these simple expressions.[16]

Another possibility for the choice of the parameters in the $E4$ operator (3.3) is to take the coefficients equal to the matrix elements of the $r^4Y^{(4)}$ operator in the *sdg* harmonic-oscillator basis,[17]

$$\alpha(l_1l_2)\sim\langle n_1l_1\|r^4Y^{(4)}(\theta,\phi)\|n_2l_2\rangle ,$$

where (n_i,l_i) stands for the quantum number of the harmonic-oscillator wave function. In this way one obtains (taking $\beta=1$)

$$\eta_1=\tfrac{19}{28}\sqrt{5},\quad \eta_2=-\tfrac{5}{14}\sqrt{11},\quad \eta_3=\tfrac{3}{28}\sqrt{11.13}\ . \tag{3.8}$$

With this $E4$ operator the following $E4$ strength distribution is calculated,

$$\begin{aligned}&\langle \text{gsb}\,|\,T(E4)\,|\,\text{gsb}\rangle^2\sim 6N^2 ,\\ &\langle \beta\,|\,T(E4)\,|\,\text{gsb}\rangle^2\sim\tfrac{1}{2}N ,\\ &\langle \gamma\,|\,T(E4)\,|\,\text{gsb}\rangle^2\sim\tfrac{5}{4}N ,\\ &\text{“others”}\equiv 0 .\end{aligned} \tag{3.9}$$

These results also follow from the fact that the operator $T(E4)$ with the parameters as given by (3.8) is a pure SU(3) (2,2) tensor, which forbids the transition from the SU(3) irreps $(4N,0)$ (ground-state band) to any irreps (λ,μ) with $\mu>2$. It is interesting to note that the values of η_i thus obtained are quite close to those in Eq. (3.7).

IV. $E4$ STRENGTH DISTRIBUTION IN A PERTURBED SU(3)

In realistic cases, the SU(3) symmetry is broken and a diagonalization in full sdg space is needed. However, for large-N values the number of basis states is prohibitively large. However, in the present investigation the qualitative features are more important than the details which will vary greatly from nucleus to nucleus. Furthermore we are interested in the $E4$ strength leading to the ground state which implies that we need to consider only one-boson excitations on the ground state. For these reasons we will use the Hartree-Bose method plus Tamm-Dancoff approximation.[18] As is stated in Ref. 18, the HB+TDA calculation gives an approximation to energies of the order $1/N$. In Sec. IV B a detailed check on the accuracy of the method is made, both for energies and wave functions. In the following we will use this method to discuss the spectra and $B(E4)$ distribution for perturbed cases.

A. The influence of the g-boson energy (ε_g) in TDA

As for the coupling between *sd* subspace and g subspace, the SU(3) limit in the standard *sd* model and the SU(3) limit in the *sdg* model are considered as two extremes. To investigate in between situations, we need a scheme in which the coupling between the two subspaces is adjustable and the smooth transition from one extreme to another is possible. This can be achieved by varying the energy of g boson, ε_g, between $\varepsilon_g=\varepsilon_d=\varepsilon_s$ [SU(3) limit of the *sdg* model] and $\varepsilon_g\gg\varepsilon_d$ (*sd* model is recovered).

To investigate the influence of ε_g numerically, the following Hamiltonian is investigated in a HB+TDA scheme

$$H=\varepsilon_g\hat{\eta}_g-\kappa Q^{(2)}\cdot Q^{(2)} , \tag{4.1}$$

where $Q^{(2)}$ stands for the SU(3) quadrupole operator [see Eq. (3.2)]. The intrinsic states are expressed as (see Appendix)

$$|\,\text{gsb}\rangle=\frac{1}{\sqrt{N!}}(\tilde{\omega}_0^\dagger)^N|\,0\rangle,\quad \text{for the ground-state+band}$$

and (4.2)

$$|\,\zeta_\mu\rangle=\zeta_\mu^\dagger\frac{1}{\sqrt{(N-1)!}}(\tilde{\omega}_0^\dagger)^{N-1}|\,0\rangle ,$$

for the excited band ,

where in the SU(3) limit $\zeta_\mu^\dagger$ stands for $\sigma_0^\dagger$, $\sigma_{\pm2}^\dagger$, $\rho_{\pm2}^\dagger$, $\rho_{\pm3}^\dagger$, $\delta_0^\dagger$, $\delta_{\pm2}^\dagger$, and $\delta_{\pm4}^\dagger$ (see Table III in the Appendix), respectively. These are appropriate to model systems in the large-N limit. The structure of the general deformed bosons can be expressed quite generally as

$$\begin{aligned}&\tilde{\omega}_0^\dagger=A_s^\omega s^\dagger+A_d^\omega d_0^\dagger+A_g^\omega g_0^\dagger ,\\ &\zeta_\mu^\dagger=A_s^\zeta s^\dagger\delta_{\mu0}+A_d^\zeta d_\mu^\dagger+A_g^\zeta g_\mu^\dagger ,\end{aligned} \tag{4.3}$$

with

$$A_s^2+A_d^2+A_g^2=1 . \tag{4.4}$$

The behavior of the coefficients $P_g^\omega=(A_g^\omega)^2$ and $P_g^\zeta=(A_g^s)^2$ as a function of ε_g using the Hamiltonian (4.1) are shown in Fig. 4. The spectra of the bandheads are shown in Fig. 5. We note that with increasing ε_g, the probability of the g boson in the ground state P_g^ω decrease

gradually. In particular, for $\varepsilon_g \simeq 0.8$ MeV, $P_g^{\omega} \simeq 0.10$, which is roughly the microscopic estimate for the probability of a G pair[3] in the wave function of the ground state. When $\varepsilon_g \geq 1.6$ MeV, the intrinsic boson excitations can be grouped in two categories: excitations of $(\sigma_0^+ \sigma_2^+ \omega_0^+)$ bosons and $(\delta_0^+ \delta_2^+ \delta_4^+ \rho_1^+ \rho_3^+)$ bosons. The first group is dominated by the *sd* bosons and corresponds to the ground-state band β, and γ bands in the *sd* IBA model, respectively; the second group consists of rather pure one-*g*-boson states and corresponds to the bands which do not exist in the *sd* IBA model. For simplicity we refer to the second group as one-*g* bands. When ε_g is large, care should be taken with the interpretation of the HB-TDA spectra since multiboson excitations (i.e., β-β or γ-γ), not calculated in TDA, can lie below some of the TDA bands.

When $\varepsilon_g \gg \varepsilon_d$ the position of the β and γ bandheads becomes independent of ε_g, whereas the bands based upon one g boson increase linearly with ε_g. To obtain a splitting between β and γ bands one needs some other symmetry breaking terms like $\varepsilon_d \hat{n}_d$.

B. The accuracy of HB+TDA

In order to get an idea about the accuracy of the TDA in the intermediate coupling region we have made a comparison with an exact calculation. Since an exact calculation requires the diagonalization of large matrices, we have limited ourselves to the case with $N=6$ bosons.

In the exact calculations the Hamiltonian was diagonalized in the m scheme using the Lanczos procedure. With this procedure only the lowest eigenstates and eigenvectors can be calculated accurately.

The comparison between the two calculations is made for a set of parameters which closely resembles those used later in the paper, $\varepsilon_d = 0.3$ MeV and $\varepsilon_g = 0.8$ MeV. The strength of the quadrupole interaction has been increased to $\kappa = 0.029$ MeV in order to locate the β and γ bands at an excitation energy of about 1 MeV. In comparing excitation energies from the two calculations it should be realized that in the TDA approach only intrinsic states are constructed and their energy therefore should be regarded as some mean energy of all levels in the band. In order to minimize the rotational energy splitting in the bands, we choose the parameters of the $L^{(1)} \cdot L^{(1)}$ force in the exact calculation such that the moment of inertia of the ground-state band is infinite, i.e., all levels are degenerate. As can be seen from Fig. 6 the positions of the β and γ bands are accurately predicted in TDA to within 100 keV. However, due to the finite value of ε_g the moment of inertia of these higher bands is different from that of the ground-state band. In addition there is some mixing between the higher-lying bands, which makes a definite band assignment impossible. The nature of the 4^+ level which lies above those of the β and γ bands is not clear. It probably should not be considered as the bandhead of a $K^{\pi}=4^+$ band since its structure resembles more that of a member of a $K^{\pi}=0^+$ band instead.

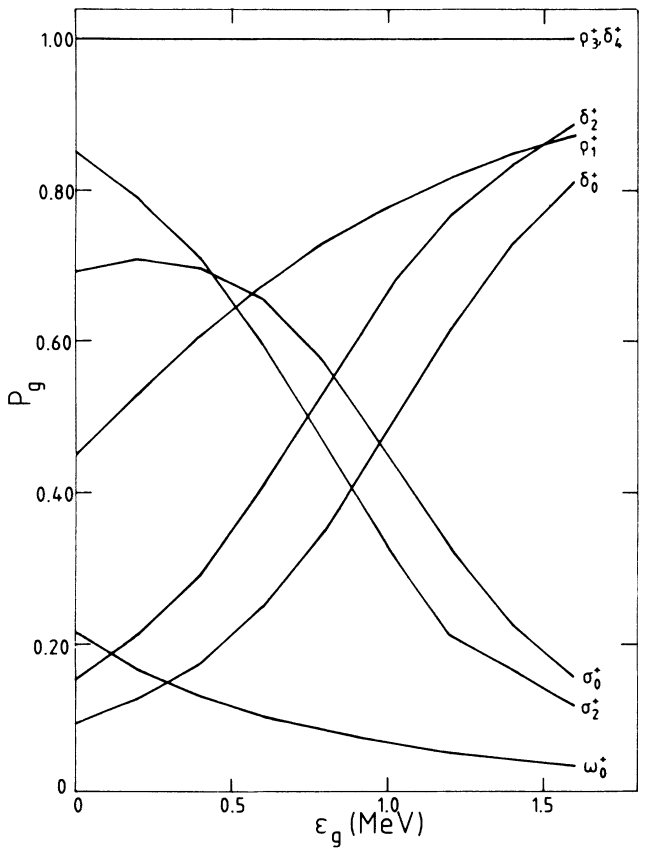

FIG. 4. The variation of the g-boson probability in the intrinsic states. The boson number is $N=14$, and the Hamiltonian is given by Eq. (4.1) with a $\kappa = 0.020$ MeV.

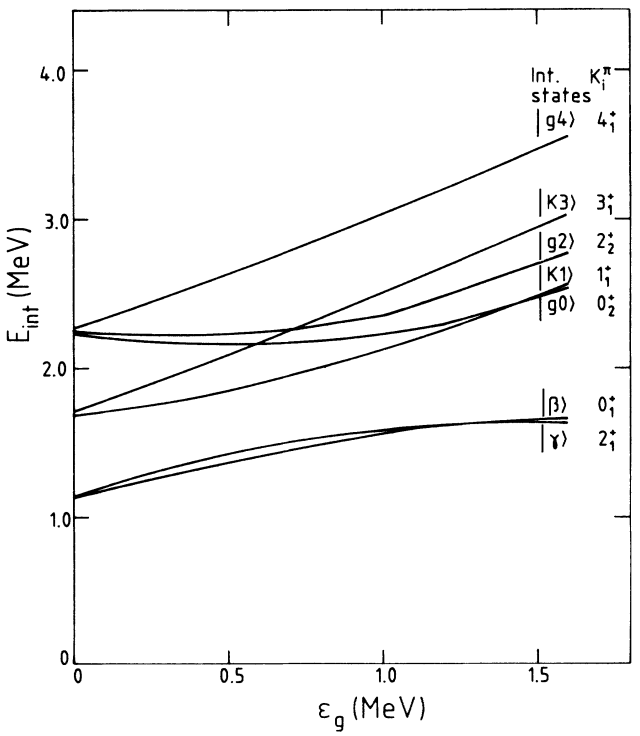

FIG. 5. The variation of one-boson-excitation bandheads. The boson number and Hamiltonian are the same as in Fig. 4.

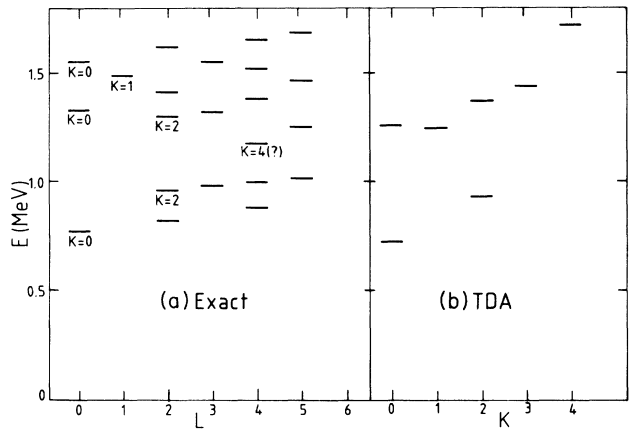

FIG. 6. A comparison between an exact calculation (complete spectrum) and TDA (bandheads only). The parameters used are in the text.

A similar comparison is made for the $E4$ and $E2$ matrix elements. We found that these matrix elements for $|\text{gsb}\rangle \rightarrow |\text{gsb}\rangle$ and $|\text{gsb}\rangle \rightarrow |\gamma\rangle$ transition in the TDA agree reasonably well with those in the exact calculation. In the exact calculation, however, the $E4$ strength to the higher-lying states is concentrated in the gamma band with very little spreading. The multiphonon configurations and the residual interaction neglected in the simple mean-filed theory have led to beta, gamma, and other bands mixing to concentrate the $E4$ strength. The $E4$ strength distribution is extremely sensitive to small changes in the Hamiltonian, either in the parameterization of $Q^{(2)}$ or in the addition of a small hexadecapole force which immediately spreads the $E4$ strength. Although this implies a caveat on trusting the TDA results, it is an extensive procedure to fit general forces to data in the shell model for large N. The band mixing matrix elements in general will scale as $N^{-1/2}$ and become generally smaller as N increases. The mean-field model should be a better approximation for $N=15$ than proven for $N=6$ in comparison with the shell model and the TDA model will be accepted for simplicity. It is clear that interpretation of TDA results, in detail, in the presence of multiphonon states is uncertain and that large scale exact calculations should incorporate a hexadecapole force for spreading stability.

C. $E4$ strengths for realistic cases

This subsection deals with the $E4$ strengths in two specific rotational nuclei ^{156}Gd and ^{150}Nd, for which systematic data on the $E4$ strengths distribution are available.[9] Since the full phenomenological *sdg* model Hamiltonian contains too many parameters we will use a Hamiltonian of the same simple form as used in the previous sections,

$$H=\varepsilon_g \hat{n}_g+\varepsilon_d \hat{n}_d-\kappa_2 Q^{(2)}\cdot Q^{(2)} . \tag{4.5}$$

For the $Q^{(2)}$ operator we have taken the SU(3) form. As an estimate we will use $\varepsilon_g \simeq 1.0$ MeV which makes the system intermediate between the SU(3) limit of the *sdg* model and the "*sd* core plus one *g* boson" picture. The κ and ε_d values are chosen such that the energy of the bandheads of the β and γ bands are reproduced. The $B(E4)$ values are calculated using the $E4$ operator of Eq. (3.5) which leaves only one adjustable parameter β. In the spectra, eight 4^+ states are given, representing the one-boson-excitation bands given by TDA. The calculated $E4$ strengths are given in Fig. 7 for ^{156}Gd and ^{150}Nd.

A comparison between experiment (Fig. 3) and calculation (Fig. 7) shows that, as far as gross feature is concerned, the agreement is reasonable for both the spectra and the $B(E4)$ strength distribution. The fragmentation of strength over many high-lying 4^+ states is reproduced. In ^{156}Gd and ^{150}Nd, ε_g and ε_d take the values 1.2,0.2 and 1.0,0.3, respectively. The experimental and calculated levels cannot be put into one-to-one correspondence, since for the higher states and the K values are unknown. It should be noted that the strength to the β band is overestimated in TDA by a considerable factor, as can be deduced from the calculations presented in Sec. IV B. This is due to residual mixing of the β and γ bands. A cranked random phase approximation (RPA) calculation is now in progress to improve upon this point.

D. The ordering of the one-*g* boson bands

For large values of ε_g, the ordering of the bands in the one-*g*-boson multiplet can be calculated by rewriting the quadrupole operator $Q_\mu^{(2)}$ as

$$Q_\mu^{(2)}=Q_{sd}^{(2)}+\tfrac{9}{7}Q_{dg}^{(2)}-\tfrac{3}{14}\sqrt{55}Q_{gg}^{(2)} , \tag{4.6a}$$

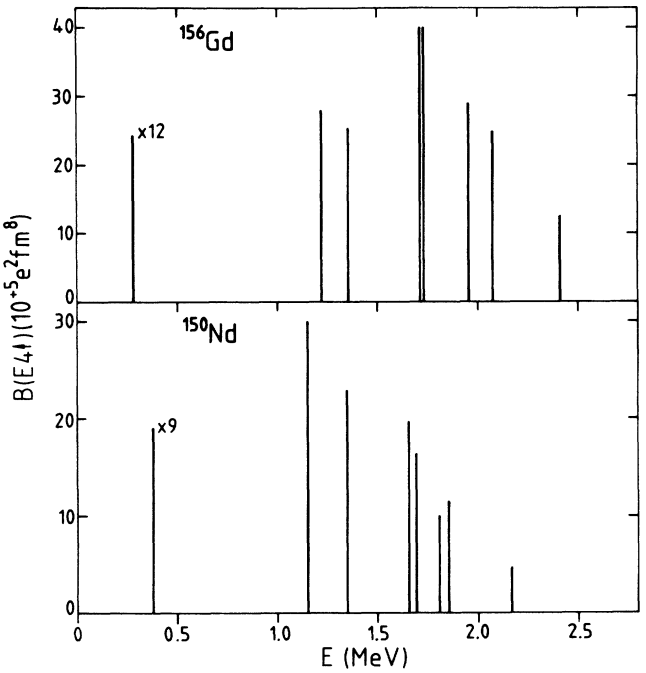

FIG. 7. The calculated 4^+ states and $B(E4)$ values in ^{156}Gd and ^{150}Nd. For ^{156}Gd the parameters $\varepsilon_d=1.2$ MeV, $\varepsilon_d=0.2$ MeV, $\kappa=0.015$ MeV, and $\beta=0.7$ have been used, while for ^{150}Nd $\varepsilon_g=0.8$ MeV, $\varepsilon_d=0.3$ MeV, $\kappa=0.0192$ MeV, and $\beta=0.0192$ MeV, and $\beta=0.75$ have been used. The $B(E4)$ value for the 4^+ state of the g.s. band must be multiplied with a factor of 12 and 9, respectively, as is indicated in the figure.

where

$$Q_{sd}^{(2)}=(d^{\dagger}\tilde{s}+s^{\dagger}\tilde{d})_{\mu}^{(2)}-\tfrac{11}{28}\sqrt{10}(d^{\dagger}\tilde{d})_{\mu}^{(2)} \tag{4.6b}$$

is very close to the quadrupole operator in the SU(3) limit of the *sd* IBA model [therefore we can use *sd* SU(3) wave function for the *sd* core], and $Q_{dg}^{(2)}$ and $Q_{gg}^{(2)}$ correspond to the $(d^{\dagger}\tilde{g}+g^{\dagger}\tilde{d})^{(2)}$ and the $(g^{\dagger}\tilde{g})^{(2)}$ terms, respectively. When $\varepsilon_g \geq 1.6$ MeV, the intrinsic wave function of the one-boson excitation can be written as

$$|\, g\times[N-1](2N-2,0)L;IM\rangle\ . \tag{4.7}$$

The splitting of the states with different K values will mainly come from the term in the Hamiltonian arising from the product of the first and third terms of Eq. (4.6a). The K dependence of the energies of the bandheads, introduced by this term is:

$$E=3.18\kappa\times 6\frac{3K^2-20}{\sqrt{7\cdot 9\cdot 11}} \tag{4.8}$$

which is of the same form as that given in Ref. 10 but with the opposite sign. The induced splitting according to Eq. (4.8) is around 0.8 MeV between the $K=0$ and the $K=4$ one-g bands in Gd. This is similar to what is shown in Fig. 6 obtained by a numerical calculation under the Tamm-Dancoff approximation.

The discussion above also shows that the pattern of the ordering of the bandheads with different K values mainly depends on the relative signs of the *sd* part and g part of the quadrupole operator (4.6a) and (4.6b). One may notice that in the ^{156}Gd case the experimental 4^+ ($E=1.462$ MeV) is not reproduced by the $Q\cdot Q$ interaction with an SU(3) $Q^{(2)}$ operator. If we choose an alternative quadrupole operator, which differs from (4.6) by an opposite sign of the $(g^{\dagger}\tilde{g})^{(2)}$ term, the overall pattern of the $E4$ strength distribution remains essentially unchanged while the 4^+ ($E=1.462$ MeV) is reproduced well. The importance of this sign can be understood in the following way: when $\varepsilon_g\sim 1.0$ MeV, the $sd+1g$ scheme is about to emerge, and the g subspace is nearly decoupled from *sd* space. The sign therefore represents the relative phase between the quadrupole deformation in the *sd* sector and that of the g sector. Whether or not the 4^+ ($E=1.462$ MeV) of ^{156}Gd is indeed a one-g-boson state is crucial for determining this relative phase. It can be checked that the opposite sign from Eq. (4.6a) corresponds to what has been assumed in the calculation of Ref. 10.

V. HEXADECAPOLE-MOMENT SYSTEMATICS

The mass (N) dependence of the hexadecapole moments β_4 in the rare-earth region is of much experimental interest.[19,20] Theoretically one has explained this N dependence in the polar cap model[19–21] and the IBA model.[22,23] Since in experiment the extracted value of β_4 is closely correlated with that of the quadrupole moment β_2, in the present paper we investigate simultaneously on a microscopic basis the N dependence of β_4 and β_2 of the ground-state band in the IBA model.

For deformed nuclei there does not yet exist a well-established mapping method to determine the boson-model parameters from a microscopic theory. Therefore, we use the schematic single-j shell model, outlined in Sec. III B and restrict ourselves to two extreme cases, the seniority scheme and fully aligned scheme.

As is discussed in Sec. III B, a mapping procedure in the seniority scheme gives rise to the $E4$ operator of the form given in Eq. (3.5). A similar result can be obtained for the $E2$ operator, the N dependence being the same as in the $E4$ operator (but with different η_i values). A simple calculation using the SU(3) wave function gives the following expectation values for quadrupole and hexadecapole-matrix elements:

$$M_2=\langle \text{gsb}\,|\,Q^{(2)}\,|\,\text{gsb}\rangle \simeq e_2 N[0.676\sqrt{\Omega-2}\sqrt{\Omega-N}+0.407(\Omega-2N)]\ , \tag{5.1a}$$

$$M_4=\langle \text{gsb}\,|\,Q^{(4)}\,|\,\text{gsb}\rangle \simeq e_4 N[0.427\sqrt{\Omega-2}\sqrt{\Omega-N}+0.864(\Omega-2N)]\ , \tag{5.1b}$$

where $\Omega=j+\frac{1}{2}$, N is the number of the nucleon pairs in the valence shell, and e_2 and e_4 are the effective charges for the quadrupole and hexadecapole moments, respectively. We note that M_4 represents the full hexadecapole moment, namely a combination of β_4 and β_2^2 which is proportional to M_2^2. Following Ref. 24 we can write, to second order in β_2:

$$\beta_4=\alpha_4 M_4-\zeta\beta_2^2=\alpha_4 M_4-\zeta\alpha_2^2 M_2^2\ , \tag{5.2}$$

ζ is the ratio between contributions to the hexadecapole-matrix elements from β_4 and β_2^2, respectively. Utilizing a geometrical model analysis[24] and neglecting the surface diffuseness correction, we have $\alpha_2=[(3/4\pi)Ze_2R_0^2]^{-1}$, $\alpha_4=[(3/4\pi)Ze_4R_0^4]^{-1}$, and $\zeta=0.7$. Choosing e_2 and e_4 such as to reproduce $(\beta_2)_{\max}$ and $(\beta_4)_{\max}$, the N dependence of β_2 and β_4 are calculated as given by the labeled curves in Fig. 8. We note that since in obtaining Eq. (5.1a) and (5.1b) an SU(3) wave function is used, the agreement of calculated N dependence with experi-

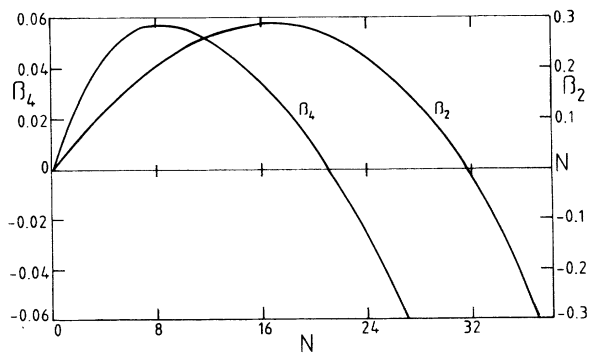

FIG. 8. Mass dependence of hexadecapole and quadrupole deformation parameters β_4 and β_2, calculated from microscopic single-j shell model in the seniority scheme.

ments[19,20] is only qualitative. The mass dependence is, however, very similar to that of the polar cap model.[21]

For a deformed system an alternative way of mapping is developed by Otsuka and co-workers.[3,25] Following the procedure given in Ref. 3, the intrinsic state for the ground-state band can be expressed as a condensate of N fermion pairs;

$$|\,\mathrm{gsb}\rangle=\eta^{-1}(\Lambda^{\dagger})^{N}|\,0\rangle\ ,$$

where the pair creation operator $\Lambda^{\dagger}$ can be expressed in terms of multipole pair creation operators

$$A_J^{\dagger}=\frac{1}{\sqrt{2}}(a_j^{\dagger}\times a_j^{\dagger})^{(J)}\ ,$$

$$\Lambda^{\dagger}=\sum_J x_J A_J^{\dagger}\ .$$

The multipole expansion parameters x_J can be obtained by minimizing the Hamiltonian. If the pairing interaction in the intrinsic Hamiltonian is neglected and a prolate shape is assumed, one finds

$$x_0\simeq\left[\frac{N}{\Omega}\right]^{1/2},$$

$$x_2\simeq(\tfrac{5}{4})^{1/2}\left[\frac{N}{\Omega}\right]^{1/2}\left[1-\frac{N}{\Omega}\right]\left[2-\frac{N}{\Omega}\right],$$

and

$$x_4\simeq(\tfrac{9}{64})\left[\frac{N}{\Omega}\right]^{1/2}\frac{\Omega^2-N^2}{\Omega^2}\,\frac{3\Omega^2-7N^2}{\Omega^2}\ . \tag{5.3}$$

The expectation value of the quadrupole and hexadecapole operator, in the intrinsic system can be expressed as

$$\langle\mathrm{gsb}\|Q_0^{(\lambda)}\|\mathrm{gsb}\rangle=\eta^{-2}\langle\Lambda^N\|Q_0^{(\lambda)}\|\Lambda^N\rangle\sim 2N(2j+1)\sum_{JJ'}\sqrt{(2J+1)(2J'+1)}\begin{bmatrix} j & j & \lambda\\ 0 & 0 & 0\end{bmatrix}\begin{Bmatrix} j & j & \lambda\\ J' & J & j\end{Bmatrix}X_JX_{J'}\ . \tag{5.4}$$

Restricting ourselves to $J,J'\leq 4$ and using Eq. (5.2), we can obtain the N dependence of both quadrupole and hexadecapole deformation parameters as given by the labeled curves in Fig. 9.

In both the seniority system and the fully aligned scheme, the N dependence of β_2 and β_4 is qualitatively reproduced from the mapping procedure. The reality of deformed nuclei is probably lying in between these two extremes, and the mass dependence of both quadrupole and hexadecapole properties can thus qualitatively be understood in a *sdg* model.

VI. OTHER OBSERVABLES

In this section we will discuss the influence of the g boson on observables that are not related to the hexadecapole operator.

A. Magnetic dipole properties

A general discussion of the structure of 1^+ levels in the *sdg*-IBA model can be found in Ref. 26. In the present paragraph we will only discuss the magnetic dipole transition strength to states of mixed neutron-proton symmetry (not studied in detail in this paper). This strength appears to depend sensitively on the g-boson content in the gsb. Barrett and Halse[27] have shown that in the SU(3) limit the inclusion of the g boson gives rise to a doubling of the $B(M1\uparrow)$ strength.

In the IBA-2 model, where neutron and proton degrees of freedom are considered explicitly, the $M1$ transition

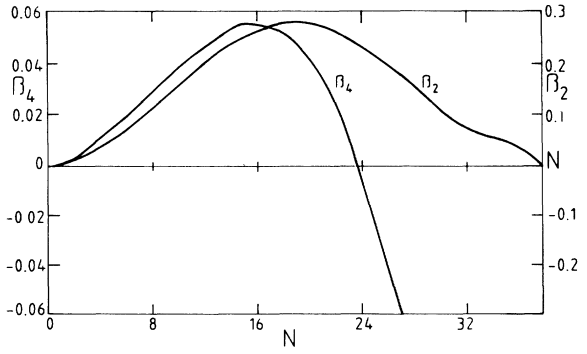

FIG. 9. Same as in Fig. 8, but the intrinsic deformed system is used to derive the mass dependence of the parameters.

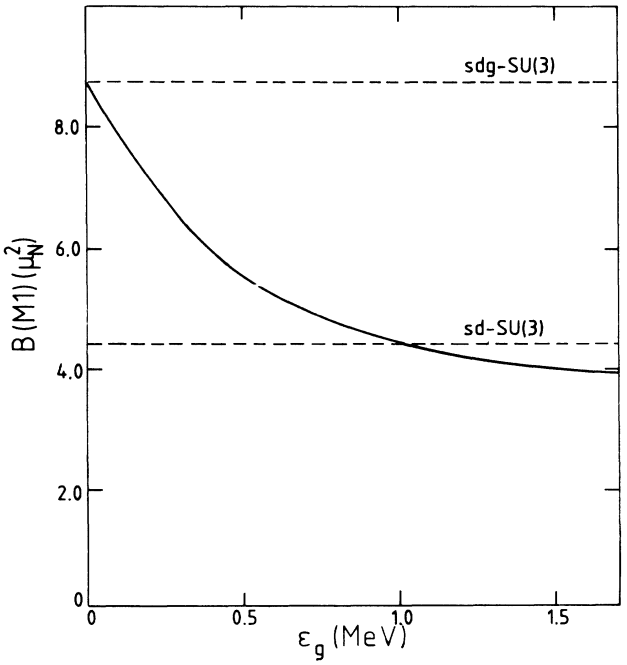

FIG. 10. The relation between $B(M1;0_1^+\rightarrow 1_{sci}^+)$ and the energy of the g boson.

TABLE II. The summed $E2$ and $E4$ strengths of ^{150}Nd.

		$\|\text{gsb}\rangle \rightarrow \|\text{gsb}\rangle$	$\|\text{gsb}\rangle \rightarrow \|\beta,\gamma\rangle$	$\|\text{gsb}\rangle \rightarrow \|\text{higher states}\rangle$
$B(E2)$	Expt.	175	7.6	7.5
(in $10^2\ e^2\text{fm}^4$)	Theor.	175	4.3	0.11
$B(E4)$	Expt.	171	3.3	85.1
(in $10^5\ e^2\text{fm}^8$)	Theor.	171	55	80.1
	(Theor.	171	17.7	89.2)

operator is given by

$$T_\mu(M1)=\sum_{\tau=\pi,\nu}\sqrt{3/4\pi}[g_{d,\tau}\sqrt{10}(d^\dagger\tilde{d}_\tau)^{(1)}_\mu + g_{g,\tau}\sqrt{60}(g^\dagger_\tau\tilde{g}_\tau)^{(1)}_\mu]\ ,$$

where g_d and g_g are the gyromagnetic ratios for $L=2$ and 4 pairs, respectively. For collective bosons the spin contribution to the magnetic moments largely cancel, yielding $g_{d,\nu}\simeq g_{g,\nu}\simeq 0$ and $g_{d,\pi}\simeq g_{g,\pi}\simeq 1\mu_N$.

In the SU(3) limit of the *sdg* model the $M1$ strength to the mixed-symmetry (scissor mode) state is[27]

$$B(M1,0^+\rightarrow 1^+_{\text{sci}})=\frac{3}{4\pi}\frac{8N_\nu N_\pi}{N}(g_\pi-g_\nu)^2(\mu_N^2)\ , \qquad (6.1)$$

where

$$g_\tau=\frac{3g_{d,\tau}+4g_{g,\tau}}{7}\quad(\tau=\pi,\nu)\ .$$

If in the case of ^{156}Gd, the free G values $g_p=1$ and $g_n=0$ are used in Eq. (6.1), an $M1$ strength about $8\mu_N^2$ is predicted, which is large compared to the experimental value ($\sim 2\mu_N^2$).

The influence of g boson on the magnetic dipole transition strength from the ground state to the scissor state (1^+_{sci}) is investigated using the Hamiltonian of Eq. (4.5) with the same parameters (ε_g, ε_d, and κ_2), as are used in reproducing the $E4$ data discussed in Sec. IV for the case of ^{156}Gd. Figure 10 shows that with the increase of ε_g, the $B(M1;0^+_1\rightarrow 1^+_{\text{sci}})$ is reduced from $\sim 8\mu_N^2$ to $\sim 4\mu_N^2$ when the energy of g boson varies from 0 to 1.6 MeV. This reduction improves the agreement with experiments considerably. The two dotted lines in Fig. 10 are the $B(M1;0^+_1\rightarrow 1^+_{\text{sci}})$ values in the SU(3) limit for the *sd* and *sdg* models, respectively. The decrease of $B(M1)$ is due to the decrease of the g-boson probability (P_g) both in the ground state and in the scissor state. Since in the calculation of Fig. 10, there is no Majorana interaction included, the position of the 1^+ levels are unrealistic, and it is not further discussed in this work.

B. $E2$ transitions

In this subsection, the pattern of the $B(E2)$ strength distribution is studied briefly and compared with that of the $B(E4)$. In Table II, the summed $E2$ and $E4$ strengths of ^{150}Nd are listed separately for three different classes: $|\text{gsb}\rangle\rightarrow|\text{gsb}\rangle$, $|\text{gsb}\rangle\rightarrow|\beta,\gamma\rangle$, and $|\text{gsb}\rightarrow|\text{higher states}\rangle$, in which "higher states" stand for the 2^+ and 4^+ states above the β and γ bands. In the experimental data excitation energies above 2.5 MeV (2^+) and 2.75 MeV (4^+), are excluded. A prominent feature of the data given in Table II is that for the transition $|\text{gsb}\rangle\rightarrow|\text{higher states}\rangle$ the $E2$ strength is negligible, whereas the $E4$ has a considerable amount of strength ($\sim 30\%$ of the total). The calculated summed $E2$ and $E4$ strengths are given for a comparison. The difference between the $B(E2)$ and $B(E4)$ strength distributions is reproduced in the calculation. As is pointed out in Sec. IV B, the $B(E4)$ strength to the 4^+_β is too large compared to exact calculation and this is partly due to the inaccuracy of TDA. If one includes a hexadecapole interaction in addition to the quadrupole one, the strength of $|\text{gsb}\rangle\rightarrow 4^+_\beta\rangle$ is considerably reduced, which is shown in the row within the parentheses in Table II. As far as the higher states are concerned, especially for the summed strength, the TDA prediction is reasonably accurate. We note that all the parameters we used for the calculation above are the same as used in Sec. IV C for ^{150}Nd reproducing the $B(E4)$ distribution. From Table II it is clear that the $E2$ and $E4$ strength distributions are qualitatively different. For the $E2$ most of the strength is concentrated in the lowest few states. In both the *sd* and *sdg* models this is reproduced since the d boson, included in the model, carries most of the $E2$ collectivity. For the $E4$ distribution much of the strength is positioned at higher energies. This, as we have shown in this paper, can only be reproduced in a model which explicitly includes a g boson, the degree of freedom that carries the $E4$ collectivity.

TABLE III. SU(3) intrinsic boson operator. This table is taken from Ref. 15.

Notation	Operator
$\omega^\dagger_0$	$\sqrt{1/5}s^\dagger+\sqrt{4/7}d^\dagger_0+\sqrt{8/35}g^\dagger_0$
$\rho^\dagger_{\pm1}$	$\pm(\sqrt{4/7}d^\dagger_{\pm1}-\sqrt{3/7}g^\dagger_{\pm1})$
$\sigma^\dagger_0$	$\sqrt{4/15}s^\dagger+\sqrt{1/21}d^\dagger_0-\sqrt{24/35}g^\dagger_0$
$\sigma^\dagger_{\pm2}$	$\sqrt{1/7}d^\dagger_{\pm2}+\sqrt{6/7}g^\dagger_{\pm}$
$\rho^\dagger_{\pm3}$	$\pm g^\dagger_{\pm3}$
$\delta^\dagger_0$	$\sqrt{8/15}s^\dagger-\sqrt{8/21}d^\dagger+\sqrt{3/35}g^\dagger_0$
$g^\dagger_{\pm2}$	$\sqrt{6/7}d^\dagger_{\pm2}-\sqrt{1/7}g^\dagger_{\pm2}$
$\delta^\dagger_{\pm4}$	$g^\dagger_{\pm4}$

TABLE IV. SU(3) intrinsic states for one boson excitation in leading order in N.

SU(3)	irreps $(\lambda,\mu)_i K$	Band	Expression
$(4N,0)$	$K=0$	$\|\text{gsb}\rangle$	$\frac{1}{\sqrt{N!}}(\omega_0^\dagger)^N\|0\rangle\equiv\|N\rangle$
$(4N-4,2)$	$K=0$	$\|\beta\rangle$	$\sigma_0^\dagger\|N-1\rangle$
	$K=2$	$\|\gamma\rangle$	$\frac{1}{\sqrt{2}}(\sigma_{+2}^\dagger+\sigma_{-2}^\dagger)\|N-1\rangle$
$(4N-6,3)$	$K=1$	$\|K_1\rangle$	$\frac{1}{\sqrt{2}}(\rho_{+1}^\dagger+\rho_{-1}^\dagger)\|N-1\rangle$
	$K=3$	$\|K_3\rangle$	$\frac{1}{\sqrt{2}}(\rho_{+3}^\dagger+\rho_{-3}^\dagger)\|N-1\rangle$
$(4N-8,4)_1$	$K=0$	$\|g_0\rangle$	$\delta_0^\dagger\|N-1\rangle$
	$K=2$	$\|g_2\rangle$	$\frac{1}{\sqrt{2}}(\delta_{+2}^\dagger+\delta_{-2}^\dagger)\|N-1\rangle$
	$K=4$	$\|g_4\rangle$	$\frac{1}{\sqrt{2}}(\delta_{+4}^\dagger+\delta_{-4}^\dagger)\|N-1\rangle$

VII. SUMMARY AND CONCLUSIONS

In this paper we have investigated the role of the g boson in several observables of the IBA model. A realistic coupling of the g boson to the s-d bosons is determined from the observed $E4$ strength distribution. To reproduce the experiment a situation intermediate between the strong and weak coupling schemes for the g boson is preferred. The percentage of g bosons in the ground state is around 10%, of the same order of magnitude as obtained from more microscopic calculations.

Including the g bosons in the basis gives rise to the prediction of relatively low-lying ($E_x\sim 1.5$ MeV) $K^\pi=4^+$ and 3^+ bands. These bands are equivalent to one-phonon excitations in a more conventional RPA language, which is in agreement with recent calculations of Soloviev.[28]

We have also shown that qualitatively the calculated mass dependence of β_4 is in agreement with experiment[20] and the polar cap model of Bertsch.[21] It has also been shown that the $B(M1\uparrow)$ strength, which has a strong dependence[27] on the number of higher L bosons included in the model space, is in good agreement with the data. The effect of including the g boson in the model space is balanced by the finite g-boson energy. Including a g boson in the model space is crucial for explaining the observed hexadecapole strength distribution. We have shown that this can be done with realistic parameters and without spoiling the agreement for other observables.

ACKNOWLEDGMENTS

We thank J. M. Schippers for his help in data taking. The help of S. Y. van der Werf in the data taking and analysis and his careful reading of the manuscript is greatly appreciated. This work was performed as part of the research program of "Stichting voor Fundamenteel Onderzoek der Materie" (FOM) which is financially supported by the "Organisatie voor Zuiver Wetenschappelijk Onderzoek" (ZWO). They also acknowledge the support by North Atlantic Treaty Organization research Grant No. RG85/0036.

APPENDIX: INTRINSIC STATES IN SU(3)

In the SU(3) limit of the *sdg* model the intrinsic states can be constructed following the procedure given in Ref. 15. First one defines intrinsic bosons as given in Table III. In terms of these intrinsic bosons, the intrinsic states can be written as in Table IV. It should be noted that in Table IV only the leading order contribution is given. Orthogonality conditions and rotational invariance will introduce $1/N$ corrections.

*Permanent address: Suzhou University, Suzhou, China.

[1]A. Arima and F. Iachello, Ann. Phys. **99**, 253 (1976); **111**, 201 (1978); **123**, 468 (1979).
[2]T. Otsuka, A. Arima, and F. Iachello, Nucl. Phys. **A309**, 1 (1978).
[3]T. Otsuka, A. Arima, and N. Yoshinaga, Phys. Rev. Lett. **48**, 387 (1982).
[4]T. Otsuka and J. Ginocchio, Phys. Rev. Lett. **55**, 276 (1985); O. Scholten *et al.*, Phys. Rev. C **34**, 1962 (1986).
[5]Ratna Raju, Phys. Rev. C **23**, 518 (1981).
[6]H. C. Wu, Phys. Lett. **110B**, 1 (1982).
[7]Y. Akiyama, Nucl. Phys. **A433**, 369 (1985).
[8]H. C. Wu, A. E. L. Dieperink, and O. Scholten, Phys. Lett. B **187**, 205 (1987).
[9]P. B. Goldhoorn *et al.*, Phys. Lett. **103B**, 291 (1981).
[10]P. van Isacker, K. Heyde, M. Waroquier, and G. Wenes, Nucl. Phys. **A380**, 383 (1982).
[11]A. G. Drentje, H. A. Enge, and S. B. Kowalski, Nucl. Instrum. Methods **122**, 485 (1974).
[12]J. M. Schippers, W. T. A. Borghols, and S. Y. van der Werf, Nucl. Instrum. Methods **A247**, 467 (1986).
[13]J. Raynal, Program ECIS (private communication).
[14]R. S. Mackintosh, Nucl. Phys. **A266**, 379 (1976); M. N. Harakeh, Program BEL, KVI Report 77i, 1981 (unpublished).
[15]H. C. Wu, A. E. L. Dieperink, and S. Pittel, Phys. Rev. C **34**, 703 (1986).
[16]J. P. Elliot, Proc. Roy. Soc. London **245**, 562 (1958); S. Pittel (private communication).
[17]O. Scholten, Phys. Rev. C **28**, 1783 (1983).
[18]J. Dukelsky *et al.*, Nucl. Phys. **A425**, 93 (1984); S. Pittel, J. Dukelsky, R. P. J. Perarro, and H. M. Sofia, Phys. Lett. **144B**, 145 (1984).
[19]D. L. Hendrie *et al.*, Phys. Lett. **26B** 127 (1968).
[20]T. Ichihara *et al.*, Phys. Lett. **B182**, 301 (1986).
[21]G. F. Bertsch, Phys. Lett. **26B**, 130 (1968).
[22]F. Todd Baker, Phys. Rev. C **32**, 1430 (1985).
[23]I. Morrison, J. Phys. G **12**, L201 (1986).
[24]A. Bohr and B. R. Mottelson, *Nuclear Structure* (Benjamin, Reading, 1975), Vol. II.
[25]T. Otsuka, Phys. Lett. **138B**, 1 (1984).
[26]S. Pittel, J. Dukeska, R. P. J. Parasso, and H. M. Sofia, Phys. Lett. **144B**, 145 (1984).
[27]B. R. Barrett and H. Halse, Phys. Lett. **155B**, 133 (1985).
[28]V. G. Soloviev, Z. Phys. A **324**, 393 (1986).